An Integrated Approach to Ligand- and Structure-Based Drug Design: Development and Application to a Series of Serine Protease Inhibitors

Orazio Nicolotti, Teresa Fabiola Miscioscia, Andrea Carotti, Francesco Leonetti, and Angelo Carotti*

Dipartimento Farmaco-Chimico, University of Bari, via Orabona 4, I-70125 bari, Italy

Received January 15, 2008

A novel approach was developed to rationally interface structure- and ligand-based drug design through the rescoring of docking poses and automated generation of molecular alignments for 3D quantitative structure−activity relationship investigations. The procedure was driven by a genetic algorithm optimizing the value of a novel fitness function, accounting simultaneously for best regressions among binding-energy docking scores and affinities and for minimal geometric deviations from properly established crystal-based binding geometry. The GRID/CPCA method, as implemented in GOLPE, was used to feature molecular determinants of ligand binding affinity for each molecular alignment. In addition, unlike standard procedures, a novel multipoint equation was adopted to predict the binding affinity of ligands in the prediction set. Selectivity was investigated through square plots reporting experimental versus recalculated binding affinities on the targets under examination. The application of our approach to the modeling of affinity data of a large series of 3-amidinophenylalanine inhibitors of thrombin, trypsin, and factor Xa generated easily interpretable and independent models with robust statistics. As a further validation study, our approach was successfully applied to a series of 3,4,7-substituted coumarins, acting as selective MAO-B inhibitors.

INTRODUCTION

The ultimate goal of quantitative structure−activity relationship (QSAR) studies is the design of new, more-active, and selective compounds. Written on paper by hand, early QSAR models were basically mathematical equations relating a limited series of theoretical and experimental physicochemical parameters to a properly measured biological activity.[1] The growing interest in QSAR and its unexplored vast potential challenged many scientists to develop newer statistical approaches and more-suitable and novel physicochemical descriptors. In this evolving scenario, 3D QSAR methods played a crucial role.[2] In particular, comparative molecular field analysis[2] (CoMFA) followed by GRID-related approaches[3] offered medicinal chemists the unique chance to visually appreciate how the variation of molecular interaction fields (MIFs), assessed by numerous chemical probes, might be related to the modulation of a specific biological response.[4] The success of 3D QSAR methods has constantly increased, as demonstrated by the large number of publications over the years.[5] However, the main drawbacks of 3D QSAR, also referred to as a ligand-based method, have been the robustness and reliability of models being strongly dependent on the adopted criteria for molecular overlay.[6,7] On the basis of some common sense rules, molecular superimposition has been conveniently performed on certain shared structural elements that represent the core structure. In contrast, the diverse chemical substituents may benefit from a greater degree of freedom, as their space torsion has been purported to explain the variance of the biological activity. Normally, useful clues for generating acceptable molecular alignments stem from analyses of low-energy conformers fitted onto rationally determined pharmacophoric points or on key functional groups of rigid and very active ligands with experimentally resolved 3D structures.[8] However, the lack of information about the exact structure of the biological counterpart and, more importantly, about the main interactions governing ligand binding has raised serious doubts on the reliability of molecular alignments for structure−activity relationship (SAR) study.[9] The final outcome is that obtaining unequivocal reproductions of 3D QSAR models is very problematic and almost impossible; thus, 3D QSAR studies seem to be useful only for the researchers who generated them.[10] Earlier applications were successfully developed on the idea of overcoming this limitation through the automatic choice of conformations and alignments of molecules. Compass[11] is probably the first example, while others deserving to be mentioned are Mimic,[12] CScore,[13] and X-CScore.[14] However, this issue still remains widely debated, as testified by other recently published papers.[15,16] Another remarkable milestone in drug design has been the foundation of the Protein Data Bank (PDB) consortium, "the single worldwide depository of information about the three-dimensional structures of large biological molecules, including proteins and nucleic acids". The PDB was established in 1971 at Brookhaven National Laboratory and today contains more than 45,000 3D structures (originally only seven) of biological molecules.[17] The immediate availability of protein structures[18] has led to the development of structure-based ligand design and new automated methods (e.g., ligand−protein docking) to simulate the binding of small molecules to their biological targets.[11–16,19] Despite the development of numerous algorithms to explore all of the energetically allowable docking poses, to select and properly rank the combinatorial number

* Corresponding author e-mail: carotti@farmchim.uniba.it.

10.1021/ci800015s CCC: $40.75 © 2008 American Chemical Society
Published on Web 06/10/2008

of possible ligand−ligate complexes, molecular docking still remains a challenging task. Although docking might easily generate misleading or futile results, it represents a general and very popular procedure for both lead identification, typically through virtual screening, and lead optimization, which is often pursued along with 3D QSAR studies.[20] For the former, the reader is referred elsewhere, since it is out of the scope of the present study. Our interest was principally directed toward the second issue and, more specifically, toward the combined use of docking and 3D QSAR methods.

The first simple, yet very pertinent, question is how to select a suitable docking pose for aligning a set of molecular ligands for 3D QSAR. To answer this question, several different strategies may be considered.[21] Preference has generally been given to selecting the top-scored docking poses on the basis of the hypothesis that the more energetically stable docking solution is the one that better represents the true ligand binding mode.[22] Alternatively, cluster analysis has been applied to group similar docking solutions with low root-mean-square deviations (RMSD); docking poses are then selected from the highest-populated conformer clusters.[23] However, acting on the sole basis of energetic or geometric data may lead to arbitrarily selecting only one solution and discarding all others generated at the expense of the elevated computational time needed to carry out all of the docking runs. In addition, the biological response values, which are the only experimentally measured values representing the dependent variable in 3D QSAR analyses, are not taken into consideration. These objective limitations prompted us to conceive a new strategy to rationally interface docking with 3D QSAR. The principles and methods underlining this strategy, as well as the results obtained by applying it to the analysis of affinity and selectivity data of a large series of benzamidine inhibitors of thrombin, trypsin, and factor Xa (fXa) will be presented and discussed herein.

Briefly, instead of undergoing a preliminary filter, all ligand−ligate complexes generated during docking simulations were rescored through a genetic algorithm[24] (GA) which optimizes a suitably developed two-component function that simultaneously computes the goodness of the regression relating docking energies with biological responses and the RMSD values calculated from a crystal-based binding hypothesis. Therefore, the ligand docking poses selected and overlaid to build the molecular alignment will be those showing both a high correlation between docking binding energy and binding affinity and a low RMSD value. A modified equation that balances the weight of large-sized chemical substituents was developed and employed to obtain more suitable measures of RMSD. The final result was the automated generation of rational molecular alignments, easily visible in the target binding site, to be used for subsequent selectivity studies and 3D QSAR analyses of serine proteases. In addition to intensive validation analyses, a multipoint equation was developed to predict binding affinities of test set inhibitors.[25] Selectivity was assessed graphing experimental and recalculated binding-affinity values in square plots. Our method was applied to the analysis of a well-known series of 88 (72 in the training and 16 in the test set, respectively) benzamidine inhibitors of thrombin, trypsin, and fXa, previously examined by Böhm et al.[26] and Murcia et al.[27] using different approaches. These serine proteases play a key role in many pathologies, carrying out a broad range of biological functions which can be significantly modified by even a small variation in their amino acid sequence, leading to subtle changes in the shape and size of the substrate-binding site. It is a known fact, for instance, that trypsin facilitates digestion, whereas thrombin and fXa are involved in the blood-clotting cascade. Although difficult and challenging, the design of selective inhibitors of these enzymes has been pursued to minimize the occurrence of cross-reactivity and side effects for anticoagulants and antithrombotic agents. Hopefully, our computational approach will aid in attaining such an important goal. For this purpose, the procedure was completely automated and implemented in a GA-based software package named *@lic&* (*ali*gning *c*hemical *e*nsembles), developed in-house.

MATERIALS AND METHODS

As in previous studies,[26,27] molecular collections of 72 and 16 3-amidinophenylalanine protease inhibitors (compounds **1**−**72** and **73**−**88**, Table 1) were used as the training and test sets, respectively, to challenge the validity and performance of the method proposed in this investigation. Structural variations of the parent structure took place at positions R1 and R2 (Figure 1 and Table 1).

As previously reported,[26,27] the protonation state of acidic and basic groups was assumed to be as follows: the benzamidine and basic amino functional groups were protonated, whereas aromatic amino functional groups were left uncharged; carboxylic groups were considered to be deprotonated. The chemical structures of benzamidine derivatives were taken from the Tripos database available for the CoMFA tutorial[28] and subjected to preliminary minimization using the standard *Premin* script released in MacroModel 9.1.[29]

The coordinates for thrombin, trypsin, and fXa were obtained from the 1ETS, [30] 1PPH,[31] and 1KYE[32] crystal structures available in the PDB. Proteins were prepared by adding hydrogen atoms, inserting and optimizing missing residues, and removing water and cocrystallized inhibitors. On the basis of documented literature,[26] controls were carefully carried out on the protonation state of polar residues leaning into the active site. Using the *Protein Preparation* module in *Maestro 7.5*,[33] implementing the *OPLS* all-atom[34] force field, light relaxation was performed to optimize hydroxyl and thiol torsions followed by all-atom constrained minimization to relieve steric clashes until the RMSD reached 0.18 Å.

The experimental inhibitory activities toward the three proteins were expressed as pK_i. It should be stressed that, while affinities for thrombin and trypsin were high and spanned a range of 4.0 and 3.4 logarithmic units, respectively, the corresponding data for fXa indicated lower affinities and a narrower spread (3.0 logarithmic units), a range that might still allow derivation of statistically significant 3D QSAR models. Pair-wise sequence comparison of the three targets was carried out with EMBOSS,[35] and values of sequence similarity, RMSD in relation to backbone α carbons, and, finally, correlation coefficients among the three sets of pK_i are listed in Table 2.

Although the proteases share the same catalytic triad formed by Asp102, His57, and Ser195, they present substantial structural differences and rendered data interpretation

Table 1. Substituents at Positions R1 and R2 and Formal Charges of the 88 Examined Inhibitors[a]

				experimental pK_i[b]			calculated pK_i[c]		
No	**R1**	**R2**	**charge**	**thr**	**trp**	**fXa**	**thr**	**trp**	**fXa**
1		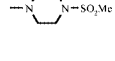	+1	8.377	6.770	5.409	8.237	6.708	5.445
2	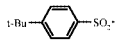	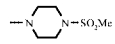	+1	8.367	6.796	5.167	8.268	6.718	4.969
3	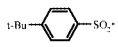	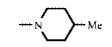	+1	8.301	6.699	4.921	7.984	6.625	4.960
4	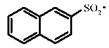	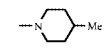	+1	8.208	6.854	4.387	7.779	6.786	4.154
5	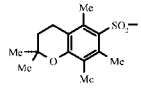	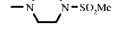	+1	8.131	6.119	4.125	8.084	6.324	4.238
6	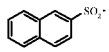	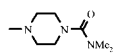	+1	8.056	6.770	4.620	8.071	6.910	4.578
7	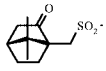	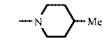	+1	7.854	6.201	4.854	7.443	6.105	4.622
8		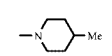	+1	7.796	6.201	4.377	7.873	6.134	3.974
9	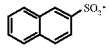	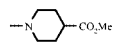	+1	7.770	7.444	4.367	7.567	6.881	4.318
10	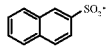	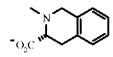	0	7.745	6.886	4.382	7.355	6.576	4.719
11	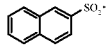	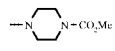	+1	7.721	7.699	4.114	7.848	6.820	4.404
12	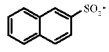		+1	7.678	6.260	4.585	7.037	6.442	4.578
13	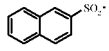	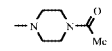	+1	7.638	6.854	4.319	7.899	6.687	4.440
14	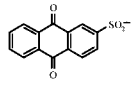	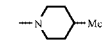	+1	7.585	7.131	5.638	6.896	6.643	5.602
15	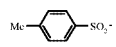	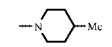	+1	7.585	6.284	4.149	7.874	6.572	3.994
16	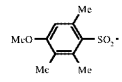	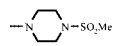	+1	7.495	5.745	3.921	7.495	6.092	3.921
17	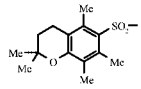	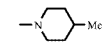	+1	7.469	6.137	4.097	7.594	6.349	4.227
18	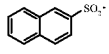		+1	7.432	6.585	4.745	7.644	6.647	4.537
19	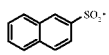	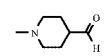	+1	7.432	6.658	4.721	6.966	6.547	4.439
20	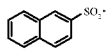		+1	7.377	6.284	5.658	6.818	6.465	5.462
21	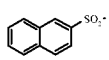		+1	7.377	6.678	4.796	6.859	6.379	4.848
22	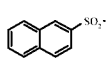	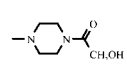	+1	7.237	5.959	4.456	7.368	6.349	4.494
23	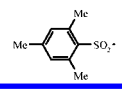	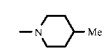	+1	7.229	5.398	4.022	7.278	5.715	3.957

Table 1. Continued

				experimental pK_i [b]			calculated pK_i [c]		
No	**R1**	**R2**	**charge**	**thr**	**trp**	**fXa**	**thr**	**trp**	**fXa**
24	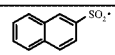		+1	7.187	6.481	4.420	7.422	6.333	4.466
25	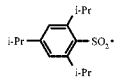	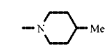	+1	7.125	6.161	5.699	7.370	5.659	5.625
26	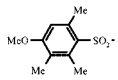	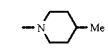	+1	7.051	6.108	4.000	7.529	6.082	4.146
27	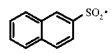	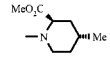	+1	7.018	5.658	4.237	6.914	6.224	4.189
28	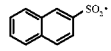		+1	6.959	5.854	5.456	6.523	5.350	5.211
29	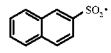	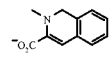	0	6.921	5.347	4.268	6.063	5.142	4.436
30	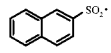		+1	6.921	5.824	5.638	6.783	6.264	5.327
31	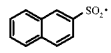	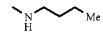	+1	6.921	5.398	4.328	6.876	5.182	4.543
32	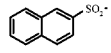		+1	6.824	6.409	4.745	6.812	6.418	4.793
33	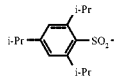	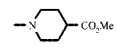	+1	6.824	6.569	5.585	6.687	6.200	5.604
34	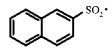	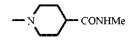	+1	6.796	6.796	4.119	7.398	6.856	4.069
35	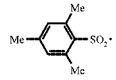	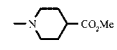	+1	6.745	6.004	4.076	6.924	6.243	3.924
36	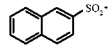	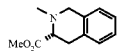	+1	6.699	5.921	4.569	6.689	6.021	4.732
37	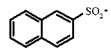	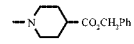	+1	6.678	7.174	5.092	6.278	7.039	4.907
38			+1	6.638	6.215	4.770	6.975	6.041	4.799
39	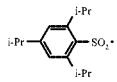	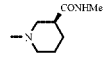	+1	6.638	6.102	5.824	6.759	6.309	5.841
40	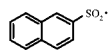		0	6.585	6.201	4.420	6.799	6.048	4.420
41	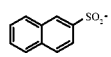		+1	6.553	5.602	5.602	5.971	4.808	5.048
42	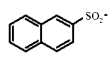	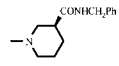	+1	6.553	6.921	4.770	6.592	6.341	4.997
43	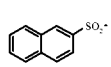		+1	6.495	5.921	4.886	6.451	6.062	4.560
44			+1	6.469	5.444	3.745	6.532	4.993	3.873
45	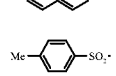		+1	6.469	5.921	4.824	6.556	6.348	4.790
46	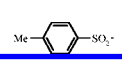		+1	6.456	5.658	4.119	6.623	5.527	4.152

Table 1. Continued

				experimental pK_i [b]			calculated pK_i [c]		
No	**R1**	**R2**	**charge**	**thr**	**trp**	**fXa**	**thr**	**trp**	**fXa**
47	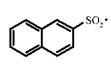		+1	6.377	5.678	5.495	6.662	6.014	5.669
48	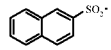		+2	6.301	6.658	4.678	6.019	6.242	4.751
49	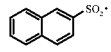	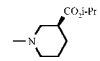	+1	6.292	6.367	4.796	6.178	6.401	4.689
50	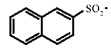	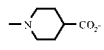	0	6.244	6.237	4.363	6.774	6.257	4.281
51	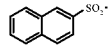		+1	6.201	6.000	4.699	6.477	6.104	4.692
52	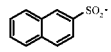		+1	6.180	5.092	3.959	6.383	5.151	4.055
53	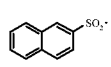	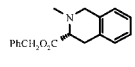	+1	6.161	5.921	5.114	6.343	6.285	5.317
54	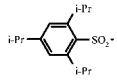	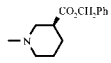	+1	6.046	6.071	6.046	6.193	6.163	6.139
55	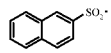		0	5.959	6.357	4.357	5.947	6.349	4.307
56			+1	5.921	4.854	4.194	6.629	5.840	4.207
57	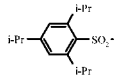	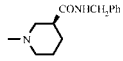	+1	5.745	6.337	5.602	6.038	6.161	5.871
58	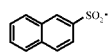	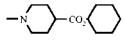	+1	5.678	7.097	5.119	5.990	6.898	5.363
59	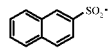		+1	5.638	5.102	4.244	5.711	5.720	4.230
60	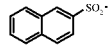		0	5.538	4.796	3.886	5.152	5.239	4.002
61	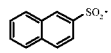	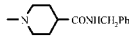	+1	5.509	6.569	4.456	5.445	6.952	4.677
62	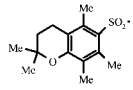		+1	5.509	4.495	5.000	5.236	4.294	4.618
63	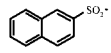		+1	5.244	4.602	4.585	5.485	4.048	4.346
64	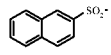		+1	5.208	4.796	3.444	5.030	4.158	3.675
65	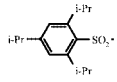		0	5.137	5.620	4.886	5.871	6.072	5.091
66		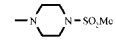	+2	4.886	4.538	3.000	4.410	4.987	3.282
67	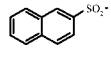	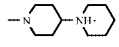	+2	4.824	6.000	4.658	4.780	5.511	4.652
68	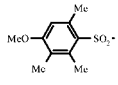		+1	4.770	3.854	3.721	4.919	4.295	3.798
69		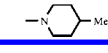	+2	4.569	4.538	3.638	4.242	4.738	3.371

Table 1. Continued

				experimental pK_i [b]			calculated pK_i [c]		
No	**R1**	**R2**	**charge**	**thr**	**trp**	**fXa**	**thr**	**trp**	**fXa**
70	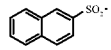		0	4.523	3.928	3.886	5.117	4.126	4.003
71	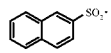	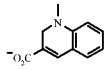	0	4.456	4.509	4.387	4.953	4.270	4.598
72	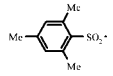		+1	4.357	3.000	3.194	4.913	3.876	3.416
73	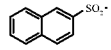	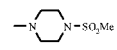	+1	8.481	6.721	4.658	6.863	6.029	4.675
74	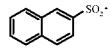	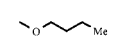	+1	7.886	6.585	5.509	6.829	5.322	4.514
75		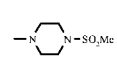	+1	7.585	6.495	5.013	7.384	6.290	4.796
76	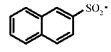		+1	7.523	6.215	4.658	7.217	6.172	4.611
77	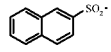	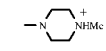	+2	7.444	5.886	4.523	7.270	6.351	4.413
78	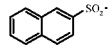		+1	7.284	6.357	4.301	6.889	5.890	4.296
79	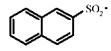		+1	7.155	5.721	4.337	6.812	6.220	4.667
80	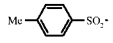		+1	6.770	6.149	4.284	6.832	6.168	4.524
81	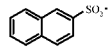	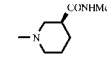	+1	6.585	6.509	4.481	6.626	6.470	4.866
82	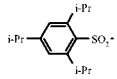	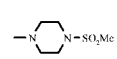	+1	6.553	6.009	5.131	6.563	5.768	5.145
83	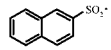	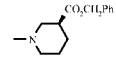	+1	6.523	6.796	5.066	6.533	6.517	4.649
84	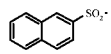	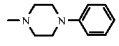	+1	6.284	7.569	4.569	6.096	6.728	4.731
85	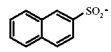		+1	6.284	5.745	4.444	6.593	6.180	4.803
86	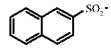	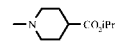	+1	6.149	7.638	4.602	5.688	6.415	4.556
87	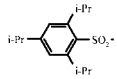		+1	5.420	4.585	4.959	6.048	4.501	4.722
88	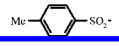		+1	4.745	4.337	4.398	6.187	4.817	3.986

[a] Experimental and calculated inhibition data for thrombin (thr), trypsin (trp), and factor Xa (fXa) are expressed as pK_i. [b] Taken from ref 26. [c] Calculated from the corresponding 3D QSAR models in Table 3.

(in Table 2) a difficult task. A higher correlation of affinity data (i.e., between thrombin and trypsin) was associated with fewer residue similarities but still good closeness of 3D structures. Aside from the S2 subsite, where the catalytic triad is located, three main additional subsites in the ligand binding pocket have been highlighted. The first, termed S1, is formed by a deep, narrow hydrophobic cavity at the bottom of which Asp189 forms a salt bridge with positively charged moieties of the inhibitor. All residues are highly conserved, apart from the A190S mutation in trypsin, whose pocket is also smaller and slightly more hydrophilic than in thrombin and fXa. The second subsite, named D (D stands for distal), is basically lined by aromatic residues and is particularly large in fXa, and smaller in trypsin and in thrombin. The other important subsite, known as P (P stands for proximal), is particularly evident in thrombin due to the insertion of

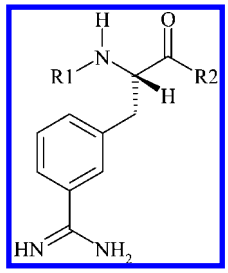

Figure 1. General structure of the examined 3-amidinophenylalanine derivatives.

Table 2. Pair-Wise Correlation among Affinity Data and Sequence/Structural Comparisons among Three Serine Proteases

target pair comparison	correlation (r)	similarity (%)	RMSD (Å)
thrombin vs trypsin	0.720	47.9	2.95
thrombin vs fXa	0.280	54.4	6.54
trypsin vs fXa	0.460	53.8	5.12

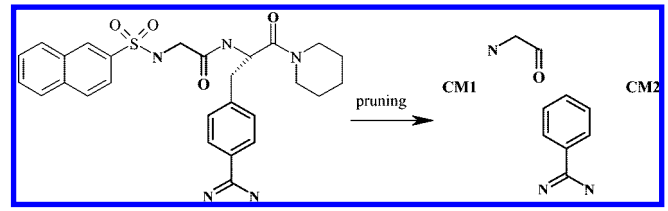

Figure 2. Crystal-based binding hypothesis generated from the 2-NAPAP−thrombin complex (PDB code 1ETS).

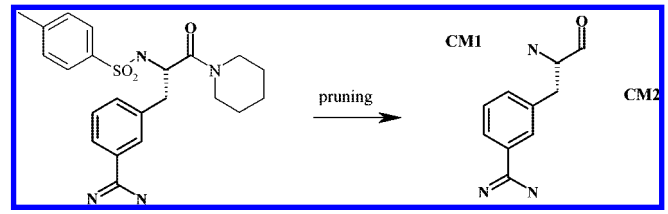

Figure 3. Crystal-based binding hypothesis generated from the 3-TAPAP−trypsin complex (PDB code 1PPH).

the loop Tyr60A−Pro60B−Pro60C−Trp60D, of low relevance in fXa and absent in trypsin. The solvent-accessible surface of these three members has been also studied, and interesting hypotheses have been set forth concerning its key role in binding affinity and selectivity.[36–38] Despite this controversial and, to some extent, confusing real-life situation, previous 3D QSAR studies have been based on the same identical molecular alignment for the three target enzymes;[26,27] hence, the resulting regression models differed only in their diverse, albeit oftentimes notably correlated (see thrombin versus trypsin), binding affinity values.

Docking Simulations and Scoring Matrices. Among the varieties of existing docking software, GOLD[39] was used for flexible ligand docking simulations, because it was extensively trained on a large number of complexes selected from the CCDC/ASTEX[40] validation set where also serine proteases, including 1PPH and 1ETS crystal structures, were represented.

While the interested reader is referred elsewhere for an in-depth discussion of the docking principles adopted in GOLD,[39,41] it has to be remarked that each docking algorithm performs better for certain protein systems than it does for others; thus, the reliability of a docking program for the target of interest must always be assessed.[42] Using GoldScore[41] as a fitness function, GOLD settings were tuned and calibrated by docking cocrystallized ligands of 1ETS, 1PPH, and 1KYE within their empty crystal structures. Expected binding modes were properly reproduced, and the lowest RMSD values, calculated for the heavy atoms between predicted and experimentally observed positions for 1ETS, 1PPH, and 1KYE, were 0.656, 1.188, and 1.118 Å, respectively. Using the refined crystal structures of thrombin, trypsin, and fXa, GOLD was set to generate 20 docking poses for each of the 72 inhibitors of the training set and 16 inhibitors of the test set. Centered on the α carbon of Gly216, residues within an active radius of 11 Å were considered in docking simulations. According to descriptions elsewhere,[27] ligand−receptor complexes were generated by setting physical constraints to favor the occurrence of well-established interactions such as the salt bridge formed by Asp189 and the hydrogen bonds (HBs) engaged by Gly216 and Gly219 with the inhibitors. Energy docking scores computed for 20 ligand−enzyme complexes originating from each of the three different serine proteases were then stored in 72 × 20 and 16 × 20 matrices for model building and external validation, respectively.

Crystal-Based Binding Hypothesis and RMSD Calculation. Several diverse but equally acceptable strategies have thus far been proposed to align molecules. For example, pharmacophoric points, resulting from knowledge-based hypotheses, and molecular templates, deriving from both rigid and active analogues, have been largely and successfully used as reference systems to superimpose other molecules. In the present study, the layout of molecular alignment for each target was taken directly from the binding geometry of the cocrystallized inhibitors of the three serine protease crystal structures used for docking. A general crystal-based binding hypothesis was then formulated by extracting Cartesian coordinates of the structural common part and by generating representative geometric centroid atoms to replace the variable regions R1 and R2 that were instead pruned.

First, Nα-[2-naphthyl-solphonyl-glycyl]-*D*,*L*-*p*-amidinophenylalanyl-piperidine (2-NAPAP), a thrombin inhibitor that, unlike all of the ligands analyzed herein, is a 4- instead of a 3-amidinophenylalanine derivative, was examined.[30] The inhibitor was extracted from the 1ETS crystal structure, limiting reading of the Cartesian coordinates to the benzamidine common part and to the inserted glycine-like spacer which was supposed to be engaged in a bidentate HB interaction with the highly conserved Gly216 of the three target enzymes. Instead, the R1 and R2 variable chains were cut out after calculating (from their Cartesian coordinates) two geometric centroid-atoms, named CM1 and CM2.

Second, the Nα-[4-toluenesolphonyl]-*D*,*L*-*m*-amidino-phenylalanyl-piperidine (3-TAPAP) trypsin inhibitor was extracted from the 1PPH crystal structure to take the Cartesian coordinates of the 3-amidinophenylalanine common part.[31] Again, the R1 and R2 variable chains were replaced by their corresponding CM1 and CM2 centroids.

Finally, the cocrystallized (*R*)-2-(3-adamantan-1-yl-ureido)-3-(3-carbamimidoyl-phenyl)-N-phenethyl-propionamide (RUP) fXa inhibitor of 1KYE was also extracted to build the crystal-based binding hypothesis for the fXa protease,[32] as described above for 3-TAPAP.

Following the procedures illustrated in Figures 2–4, 1760 (i.e., 88 × 20) docking-based binding hypotheses were

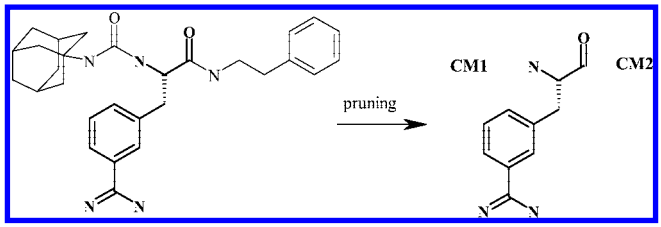

Figure 4. Crystal-based binding hypothesis generated from the RUP−fXa complex (PDB code 1KYE).

automatically generated for each target protein by properly handling each of the 20 generated docking poses. By using in-house scripts, RMSD values were computed by means of pairwise comparisons of the atoms in the crystal-based and each docking-based binding hypothesis for the three serine protease targets. To smooth the effect of overweighting large chemical substituents in establishing centroid-atom locations, size-based coefficients ($\sqrt{n_{CM}}$) were implemented, and the RMSD was calculated as follows:

$$\mathrm{RMSD} = \sqrt{\frac{\sum d^2_{\mathrm{core}} + \sqrt{n_{\mathrm{CM1}}} \times d^2_{\mathrm{CM1}} + \sqrt{n_{\mathrm{CM2}}} \times d^2_{\mathrm{CM2}}}{n_{\mathrm{tot}}}} \quad (1)$$

where d_{core} is the distances between all of the core atoms; d_{CM1} and d_{CM2} represent the distances between the centroid atoms; and n_{tot}, n_{CM1}, and n_{CM2} correspond to the number of heavy atoms forming each given benzamidine derivative and its associated chemical substituents R1 and R2, respectively. As was done for the energy docking data, the RMSD values from the training and test set were collected into 72 × 20 and 16 × 20 matrices for rescoring through *@lic&* and making predictions, respectively.

Genetic Algorithms for Docking Pose Selection. The interested reader is referred to elsewhere for an in-depth discussion on GAs[24] and to some of our recent works[25,43] to get exact details of our in-house-developed GA. Here, some useful indications are instead given to explain how our proposed fitness function operates to select docking poses. Indicated by *@fit*, it ranges from 0 to 2 to rank each theoretical molecular alignment and is based on the combination of two terms calculated as follows:

$$@fit = r^2_{s,\mathrm{p}K_i} + \frac{1}{1 + \mathrm{RMSD}_{\mathrm{avg},j}} \quad (2)$$

The first term ($r^2_{s,\mathrm{p}K_i}$) will tend toward 1 when scouting the best possible regression between binding affinity and docking score values. The second term ($1/(1 + \mathrm{RMSD}_{\mathrm{avg},j})$) will also converge to 1 when the RMSD value drops to zero. In an ideal situation, optimal molecular alignment should display a perfect linear relationship between biological and docking score values ($r^2_{s,\mathrm{p}K_i} = 1$) and also complete structural overlay ($\mathrm{RMSD}_{\mathrm{avg},j} = 0$); in such an ideal case, the *@fit* function will achieve its maximum, which equals 2. However, valuable real-life models should be provided with a high $r^2_{s,\mathrm{p}K_i}$ and a low RMSD value.

3D QSAR Methods. Compounds included in our automated molecular alignments were analyzed using GRID to obtain MIFs with five representative probes (DRY, N1+, N1, O, and OH) typifying hydrophobic, electrostatic, HB donor, HB acceptor, and HB acceptor/donor groups, respectively, and to survey the main physicochemical features of the inhibitors, as shown in previous studies on the same targets.[44] Generally adopted to describe and evaluate differences (and, thus, selectivity) among various proteins (e.g., serine proteases, penicillin acylases, and dihydrofolate reductases),[45,46] consensus principal component analysis (CPCA) was used to explain the overall variance of the probe matrix by means of a two-level analysis. As reported in the original work, the block level represents the *opinion* of each block of variables, whereas the superlevel expresses the *consensus* of all blocks. The combined use of GRID/CPCA in our study allowed characterization of the main structural differences of the three molecular overlays extracted by *@lic&* during rescoring of the docking results. Analysis of the MIFs was conducted with GOLPE,[47] an advanced statistical tool used for both variable selection and model validation, where the field matrix was unfolded to produce one-dimensional vector variables for each compound. The original matrix with field values was then pretreated to select unbiased variables by zeroing the positive and negative ones and applying a standard deviation cutoff. The N level was set and the weighting procedure, known as block unscaled weights, was adopted to normalize the importance of each block of variables, particularly the DRY MIFs, by scaling each block separately, whereas the scales of single variables within each block remained unchanged. After selecting relevant probes, partial least-squares (PLS) analyses were performed with the leave-one-out cross-validation procedure.[48] The optimal number of components (ONC) in the PLS models was considered the one yielding the smallest standard deviation error in prediction (SDEP), given that the increase of q^2 was not higher than 5% when adding another component. In all of the cases analyzed, the smart region definition algorithm was used to group variables (number of seeds = 1500, critical distance = 1.0 Å, collapsing cutoff = 2.0 Å) and two fractional factorial design variable selection runs were then executed to obtain the final 3D QSAR model.[49]

Multipoint Predictive Equation. Correctly predicting the binding affinity values of new compounds before their actual synthesis is the ultimate goal of any 3D QSAR study.[25] Typically used for validation, predictions in 3D QSAR are performed on a test set consisting of a limited number of compounds extracted from the entire data set according to widely accepted criteria based on structural diversity and regular distribution of activity values. Although highly sensitive to geometry and spatial orientation, predicted values are calculated from only one possible conformer which, most of the time, is manually modeled on the basis of similar compounds in the training set. The rationale behind this criterion could, however, be often suspicious and questionable.[9,10] In the present work, a phenomenological approach was employed for deriving more appropriate and reliable predictions. The predicted binding affinity of each *i*th compound in the test set (**73**−**88** of Table 1) was calculated as a weighted arithmetic mean that combines predicted binding affinity values of each *j*th (from 1 to 20) individual docking solution with a series of computed coefficients, as follows:

$$\bar{pK}_{i,pred} = \frac{\sum_{j=1}^{20} (pK_{i,j} \times w_j^m)}{\sum_{j=1}^{20} w_j^m} \quad (3)$$

where $pK_{i,j}$ and w_j indicate the predicted binding affinity and its corresponding coefficient, respectively, while the value of m was assigned by calibration. Determination of w_j loading was performed according to a weighting scheme awarding solutions with high docking scores and small deviations from the crystal-based binding hypothesis, as follows:

$$w_j = C + A_j + (1 - B_j) \quad (4)$$

where C is a numerical constant normally set to 1 to ensure the proper exploration of w_j at the change of m, whereas A_j and B_j represent the 0−1 normalized data relative to docking scores and RMSDs, calculated according to the crystal-based binding hypothesis of each individual jth conformer of the test set. The above equation discloses the putative competitive nature of A_j and B_j.[50] In fact, the loading of w_j would reach its maximum in the optimal situation where A_j and B_j are simultaneously equal to 1 and 0, respectively, and its minimum in the worst case where A_j and B_j concomitantly assume the values of 0 and 1, respectively. Whenever better predictions arose when considering docking scores or, alternatively, only RMSD values, the entire A or B jth array would drop to 0 and 1. The optimal value of the m exponent, however, was empirically determined by intersecting the minimum of the average sum of predicted absolute residuals (ASPAR) of test set compounds:

$$\text{ASPAR} = \frac{\sum_{i=73}^{88} |pK_{i,obs} - \bar{pK}_{i,pred}|}{n_{test}} \quad (5)$$

where $pK_{i,obs}$, $\bar{pK}_{i,pred}$, and n_{test} represent the observed and predicted pK_i values and the number of compounds in the test set, respectively. In the simplest case (i.e., when $m = 0$), the multipoint prediction equation yielded the more common arithmetic mean. We generally observed (see later text) that single-point prediction based on top-scored or bottom-RMSD docking poses generally did not yield better results than the multipoint approach based on the weighted mean (i.e., when $m \neq 0$ and ASPAR is minimal).

Description of Software. *@lic&*, written in Matlab code,[51] is a customizable toolbox available as a stand-alone system or with a user-friendly interface. Aside from the options already described for rescoring docking poses and to automatically generate molecular alignments for 3D QSAR, *@lic&* provides many additional features. Briefly, diverse numerical coefficients can be associated to the two terms of the *@fit* fitness function, or alternatively, the molecular alignment may be driven also by the energy or geometric term only. Parameters for the GA runs are also user-adjustable according to the complexity of the molecular overlay. In particular, the user can select the multiple population option. Statistical tools are implemented to display regression plots and matrix heat maps, and a PyMOL interface add-on is internally available for visual inspection.[52] In our laboratory, *@lic&* was usually run on a Pentium 4, 2.6 GHz PC with 1 GB of RAM and on a 5-node Cluster Linux openMosix (AMD Athlon XP 2400+ CPUs). Three different and independent populations were employed for the evolutionary search with the number of individuals doubling the number of compounds in the training set. Mutation and crossover genetic operators were set at 0.1 and 0.9, respectively. *@lic&* required about 6 h of computing time to perform 10^6 iterations on a Pentium PC during analysis of the serine protease inhibitors.

RESULTS AND DISCUSSION

The pool of 20 docking solutions per ligand, generated by GOLD for each serine protease, was separately rescored to build the molecular alignments for 3D QSAR analyses. Three inputs were submitted to *@lic&*: the biological vector containing the 72 experimentally determined pK_i values, two 72×20 matrices containing the docking energy scores from GOLD, and the RMSD values calculated on the basis of the crystal-based binding hypotheses.

Validation, Prediction, and Selectivity. Before discussing the chemical interpretability of 3D QSAR models derived from our automated alignments by surveying the main physicochemical features modulating biological affinity, models needed to be analyzed first in terms of validation to verify that their statistics were not due to chance correlation,[10] then in terms of prediction to line their domain of biochemical applicability,[50] and ultimately in terms of selectivity to prove their ability to distinguish diverse proteins.[53] A number of different validation analyses can be applied, such as y-scrambling and randomized roto-translation of selected docking solutions. In addition to these (see the Supporting Information), baseline 3D QSAR models were considered, which resulted from the selection of top-scored or bottom-RMSD conformers in each docking run, as routinely done in the past in docking-based 3D QSAR studies. To our satisfaction, the q^2 values in Table 3 unequivocally indicated that our models outnumbered the statistics of baseline models in all cases, an improvement which was more evident when comparing the top-scored models. Finally, to better prove the general validity and applicability of our method, an additional series of 54 3,4,7-substituted coumarins displaying a selective MAO-B inhibition[20,54,55] was successfully analyzed. Models with good fitting and predictive power were obtained. A brief discussion of the results and further methodological details are given in the Supporting Information.

The structure−activity portability of our 3D QSAR models was challenged by predicting pK_i values of inhibitors comprised in the test set (**73**−**88** in Table 1). In the interest of science, it must be stated that a relationship between internal and external predictions has never been proved, and very often, high internal predictability may correspond to low external predictability, and vice versa. This dilemma, also known as *Kubinyi's paradox*, represents one of the ultimate and perhaps unsolvable issues for QSAR practitioners.[56]

In the present study, external predictions were made through a multipoint predictive equation upon determination of an appropriate value of m on the basis of a lower ASPAR value. In the case of thrombin and trypsin inhibitors, the best overall predictions were obtained setting m to 6 and 10, respectively. The comparisons between experimental and predicted pK_i yielded satisfying values of predictive squared

Table 3. GRID-GOLPE Statistics for *@fit*, Top-Scored, and Bottom-RMSD Alignments for the Indicated MIFs[a]

target	MIF	alignment	*@fit*	$r^2_{s,pKi}$	$RMSD_{avg}$	ONC	q^2	SDEP	r^2	SDEC
Thrombin, 1ETS	DRY OH	*@fit*-model	1.111	0.735	1.661		0.777	0.343	0.887	0.484
		top-scored	0.422	0.084	1.962	1	0.298	0.526	0.932	0.297
		bottom-RMSD	0.500	0.034	1.152		0.624	0.628	0.805	0.452
trypsin, 1PPH	DRY N1 O	*@fit*-model	1.232	0.742	1.039		0.752	0.368	0.823	0.436
		top-scored	0.552	0.160	1.550	1	0.336	0.461	0.885	0.297
		bottom-RMSD	0.696	0.090	0.649		0.696	0.482	0.859	0.328
fXa, 1KYE	DRY N1 O	*@fit*-model	0.969	0.595	1.664		0.728	0.330	0.914	0.185
		top-scored	0.352	10^{-4}	1.839	2	0.356	0.507	0.736	0.325
		bottom-RMSD	0.496	0.021	1.104		0.503	0.446	0.795	0.287

[a] Alignments labeled as *@fit*-model were determined on the basis of the *@fit* fitness function, whereas those indicated as top-scored and bottom-RMSD represent baseline models computed by picking up docking poses with the best docking energy and lowest RMSD values, respectively. *@fit*, $r^2_{s,pKi}$, and $RMSD_{avg}$ represent the *@fit* fitness value, the squared correlation coefficient, and the averaged sum of RMSD calculated by *@lic&*. ONC indicates the optimal number of PLS components, while q^2, SDEC, r^2, and SDEP represent the leave-one-out cross-validated correlation, the standard deviation error in calculation, the squared correlation coefficient, and the standard deviation error in prediction, respectively.

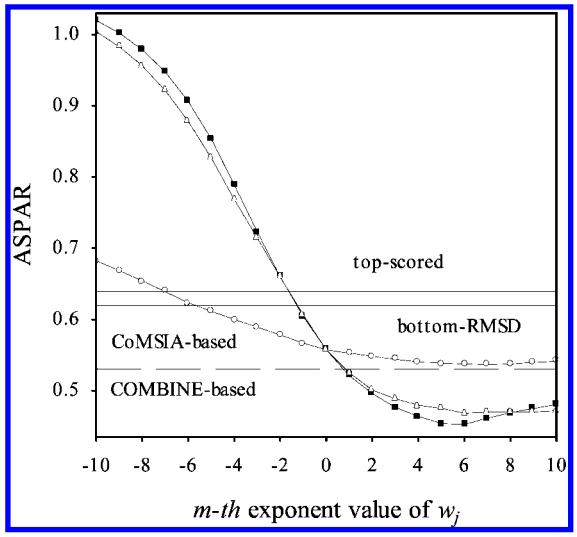

Figure 5. Plot of the ASPAR values of thrombin inhibitors versus the *m*th exponent value of w_j. Dashed lines labelled with COMBINE and CoMSIA came from previously published data, whereas continuous top-scored and bottom-RMSD lines were associated with our baseline models. Squares, triangles, and circles were instead referred to our multipoint predictive equation where w_j accounted for A_j and B_j simultaneously and for A_j or B_j only.

correlation coefficient r^2_{pred}, equalling 0.554 and 0.588 for thrombin and trypsin, respectively, while for previously applied approaches, such as CoMSIA[26] and COMBINE,[27,57] r^2_{pred} equalled 0.432 and 0.452 for thrombin and 0.842 and 0.426 for trypsin, respectively. Moreover, a closer look at the plot in Figure 5 indicates that the multipoint equation functioned better than the single-point equation, on the basis of the top-scored or bottom-RMSD docking poses of thrombin inhibitors. This observation holds true for trypsin inhibitors as well (data not shown). In addition, it should be noted that, in the case of thrombin inhibitors, our predictive equation provided a better ASPAR value of 0.453, whereas the corresponding values for the previously used CoMSIA and COMBINE were 0.531 and 0.529, respectively. A different situation, however, was observed when predicting trypsin binding affinity. By using the same structural alignment of thrombin inhibitors, CoMSIA produced a better ASPAR value (0.264), whereas COMBINE generated a worse value (0.516); the multipoint equation applied to our independent molecular overlay directly fitted from the trypsin receptor yielded an intermediate ASPAR value of 0.455.

A careful analysis of previous reports on affinity predictions for the test set revealed that inhibitor **87** has not been included into any COMBINE calculation. Moreover, predicted thrombin affinity values of inhibitors **82** and **86** have not been quoted. Affinity prediction for inhibitor **82** was also unaccounted for in the case of fXa. In comparison with CoMSIA, our trypsin model failed to correctly predict the affinity of two compounds. Ester **74**, bearing a butoxy chain in R2, revealed a predicted pK_i of 5.322, whereas for the compound under investigation, the observed value was unexpectedly much higher at 6.585. The probable reason for such a discrepancy could be that the molecule most structurally resembling **74** in the training set was its bioisoster **31**, which bore a butylamine in R2 and an experimental pK_i value of 5.938 that was recalculated by our model to 5.182. It is worth noting that both R2 substituents exhibited a higher conformational mobility compared to all of the others; this specific feature might have not been properly accounted for in our model. The second-worse-predicted inhibitor was compound **86**, for which no valid explanation was possible.

The selectivity of a ligand depends on its ability to discriminate among various biological targets; thus, a selective compound should exert divergent affinities for distinct receptors.[58] Accordingly, it may be expected that highly selective inhibitors should contact nonconserved amino acid residues, whereas nonselective inhibitors should interact mainly with highly conserved amino acid side chains or a backbone. In this view, model selectivity should be generally investigated by relating the differences in binding affinity (e.g., between thrombin and trypsin pK_i values) with MIF variance, which is, however, normally derived from only one biased and subjective structural alignment. This procedure has allowed the obtainment of selectivity maps resulting from PLS analysis derived substantially from pK_i differences, which could propagate the experimental uncertainty of each independent biological measure. In the present investigation, selectivity was based on the assumption that two affinity models, originating from different pK_i and molecular overlays, should yield two recalculated affinity values whose difference should better match the experimental selectivity data. In our opinion, such an approach might allow for overcoming the implicit limitations of selectivity studies that did not explicitly consider the likely occurrence of non-

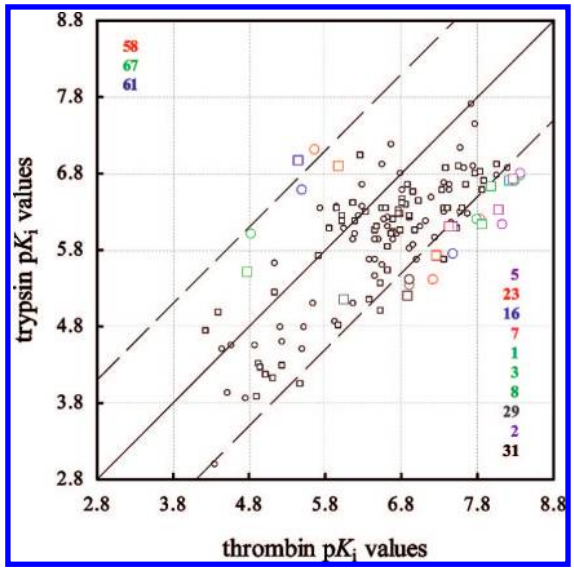

Figure 6. Selectivity square plot representing, for each compound, projections of observed versus recalculated values of thrombin and trypsin binding affinities, represented by circles and squares, respectively. Dashed lines below and above the bisectrix were drawn to better identify the more thrombin- and trypsin-selective inhibitors, respectively.

equivalent interactions of diversely oriented inhibitors into the active sites of two distinct proteins.

A straightforward analysis of selectivity data was performed by simultaneously reporting (in a square plot) thrombin versus trypsin experimental and recalculated affinities according to their corresponding 3D QSAR models (Table 3). As illustrated in Figure 6, nonselective inhibitors, characterized by equal or close pK_i values for the two targeted enzymes, were located near the bisectrix, which is the geometric locus of equally active inhibitors. At a convenient distance of 1.3 logarithmic units (corresponding to an affinity ratio of 20), two parallel dashed lines were drawn above and below the bisectrix, which was bordered by highly potent and selective thrombin and trypsin inhibitors (bottom-right and top-left corners, respectively). The decreasing selectivity of inhibitors **5**, **23**, **16**, **7**, **3**, and **2** toward thrombin was well-explained, and only a limited distance, indicative of a good recalculation, was observed between equally colored circles and squares representing pairs of experimental and recalculated differences, respectively.

The highest thrombin selectivity disclosed by inhibitor **5** was likely due to the Q192E mutation in thrombin compared to trypsin.[44] In fact, although small Cartesian variations were observed between the two conformers selected by *@lic&* from docking solutions in thrombin and trypsin, the presence and diverse orientation of Glu192 (Figure 7) in the case of the 1ETS crystal provide a strong HB acceptor group to the thrombin-selective conformer in addition to the carbonyl of Gly216. Interestingly, the molecular selectivity of inhibitor **5** was in agreement with the docking score energy assigned by GOLD to the thrombin (−53.08 kJ/mol) and trypsin (−48.20 kJ/mol) complexes selected by *@lic&*. Notably, the experimental affinity of inhibitor **5** toward thrombin and trypsin was properly recalculated from the corresponding 3D QSAR models. In fact, accurate recalculated pK_i values of 8.084 and 6.324 were obtained for thrombin and trypsin affinity, respectively, whereas the corresponding experimental values were 8.131 and 6.119. The second-best selective thrombin inhibitor, **23**, showed two different orientations for the 2,4,6-trimethyl-phenylsolphonyl substituent in R1 in the thrombin and trypsin binding sites. In thrombin, the substituent was involved in favorable hydrophobic contacts with the methylene chain of Glu217 compared to the E217S mutation[44] in trypsin of this active site region, which seemed to push away the R1 substituent of the inactive trypsin conformer. These findings were supported by the different interaction energies observed for the two complexes, that is, −61.46 kJ/mol and −54.46 kJ/mol for thrombin and trypsin, respectively. 3D QSAR models correctly recalculated pK_i values of **23** as equal to 7.278 and 5.715 for thrombin and trypsin enzymes, respectively, compared to the measured binding affinities of 7.229 and 5.398. A slight discrepancy, however, was observed in the recalculation of the thrombin selectivity of **29**, whose cyan circle and square symbols were distant by 0.653 logarithmic units. This deviating number was derived mainly from an underestimation (0.858 logarithmic units) of thrombin affinity. Reasonable recalculations were again observed for the trypsin-selective compounds **58**, **67**, and **61**.

Only more general remarks and observations could be made on selectivity data from the other two target pairs, those being thrombin/fXa and trypsin/fXa, because affinity for one of the two targets (i.e., fXa) was indeed too low. High thrombin/fXa selectivity was observed for inhibitors bearing at R2 unsubstituted pyrrolidine and azepine rings and for 4-methyl-piperidine and piperazine carrying at N4 medium-sized hydrophilic substituents. The lowest selectivity was seen for piperidine derivatives with charged groups or bulky substituents at position 3. As far as the trypsin/fXa selectivity is concerned, no clear substituent effects emerged at position 4 of the piperidine and piperazine rings in R2. Interestingly, one might notice that 16 out of the first 20 more trypsin-selective inhibitors showed at R1 the β-naphthylsulfonyl substituent. The lowest trypsin/fXa-, or even slightly fXa-, selective inhibitors were characterized by the presence of small substituents (i.e., NHMe and OMe) at R2.

Thrombin/trypsin selectivity was analyzed and predicted also for the test set compounds. Although very intriguing, this external analysis is very sensitive to all of the issues raised by *Kubinyi's paradox*. Bearing this in mind, our models continued to yield acceptable predictions of the thrombin/trypsin selectivity observed for compounds **75**, **76**, and **78** and of the reversed selective trypsin/thrombin inhibition of compounds **84** and **86**. Conversely, a disappointing prediction resulted for selective thrombin inhibitor **73**. It should be emphasized, however, that selectivity inversion was never observed for any of our targets. Similar considerations hold true also in the case of thrombin/fXa and trypsin/fXa selectivity. The square plot constructed by graphing predicted affinity values previously obtained by other authors disclosed comparable or inferior results; however, inversion of selectivity was occasionally observed.

3D QSAR Models for Thrombin Inhibition. Docking poses generated from the 1ETS refined crystal structure were rescored by *@lic&*, after which automated alignment was obtained and analyzed. A careful inspection of the GRID maps in Figure 8 demonstrates how the inhibition of thrombin was related to the structural variation in compounds **1**−**72** of the training set (Table 1). For ease of interpretation, a cyan and yellow color code was used to highlight favorable

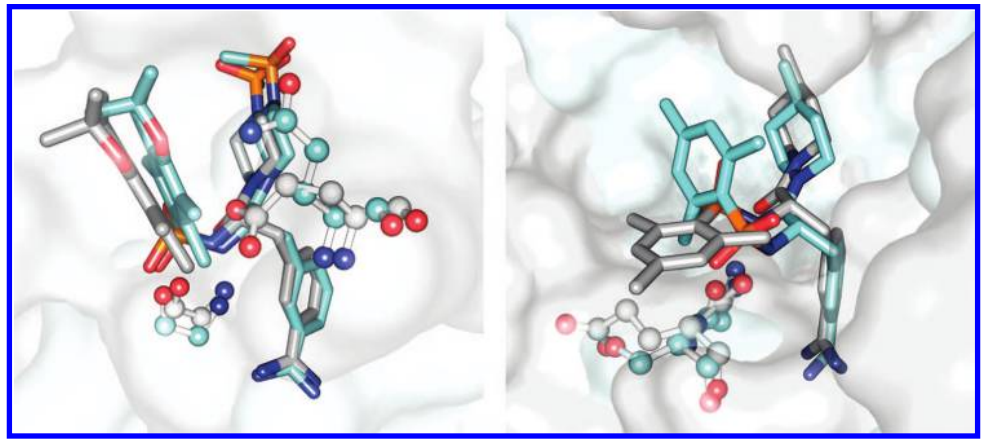

Figure 7. Thrombin and trypsin surfaces and relevant amino acid residues along with the corresponding docking solutions selected by *@lic&* are colored in white and cyan, respectively. On the left-hand side, the docking poses of the best thrombin-selective inhibitor **5**, the conserved Gly216, and the mutated Q192E residues are shown. On the right-hand side, the docking poses of the second-best thrombin-selective inhibitor **23** and the mutated S217E residues are shown.

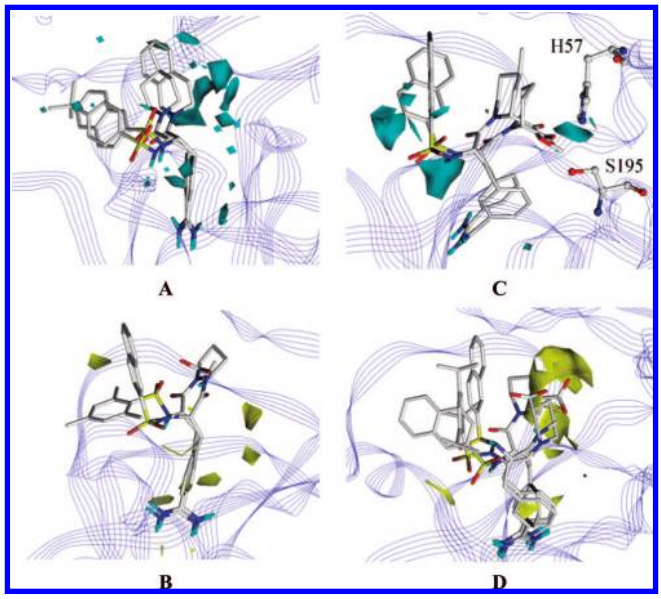

Figure 8. GRID maps for thrombin inhibitors. (A) DRY probe: favorable cyan areas were contoured at −0.0016 for active thrombin inhibitors **3** ($pK_i = 8.301$) and **18** ($pK_i = 7.432$). (B) DRY probe: unfavorable yellow areas were contoured at 0.0017 for inactive thrombin inhibitors **60** ($pK_i = 5.538$) and **72** ($pK_i = 4.357$). (C) OH probe: favorable cyan areas were contoured at −0.0016 for active thrombin inhibitors **27** ($pK_i = 7.018$) and **40** ($pK_i = 6.585$). (D) OH probe: unfavorable yellow areas were contoured at 0.0026 for inactive thrombin inhibitors **55** ($pK_i = 5.959$), **63** ($pK_i = 5.244$), and **65** ($pK_i = 5.137$).

and unfavorable interactions, respectively, for all of the examined GRID probes.

The benzamidine common core was generally embedded in the S1 subsite, whereas the R1 and R2 substituents were oriented toward the characteristic hydrophobic D and P susbites, respectively. On the basis of our automated alignment, five different MIFs were initially calculated within GRID. The most significant MIFs, DRY and OH, were selected by applying CPCA and were efficaciously used for building the 3D QSAR model with GOLPE. DRY probe analysis revealed that R1 substituents were stacked into the D region, whereas those of R2, such as the 4-methylpiperidinyl of **3** and the 1,2,3,4-tetrahydro-isoquinolinyl of **18**, were buried in the P hydrophobic subsite, a specific thrombin feature among the three serine proteases, highlighted by an evident cyan polyhedron in Figure 8. Bulky hydrophobic substituents of weakly active or inactive thrombin inhibitors, such as **60** and **72**, were intercepted by a forbidden yellow polyhedron matching part of the solvent-exposed surface.

MIFs generated through the OH probe scanned the likely occurrence of HBs. Interestingly, the well-known relevance for molecular recognition of the HB formed by the sulfonyl group in R1 with Gly219 was confirmed by a favorable cyan area. The lack of HB acceptor groups in inhibitors **56**, **66**, and **69** led to a strong decrement of activity. Moreover, considering the naphthalene ring of the R1 substituents, the greater inaccessibility to substituents in the α rather than in the β position made the β-substituted congeners more active (i.e., **4** > **8** and **24** > **38**). Polar groups at position 2 or 3 of the piperidine ring in R2 were contoured by forbidden/permitted yellow/cyan maps, as occurred for inactive (**55** and **65**) and active (**27** and **40**) inhibitors, respectively. For example, thrombin inhibitor **40**, which was functionalized with a carboxylate group, was likely to be involved in positive interactions with Ser195 and His57 belonging to the catalytic triad. In addition, HB donor groups in R2, such as the NHMe of **63**, impacted unfavorable yellow areas.

3D QSAR Models for Trypsin Inhibition. After performing docking on the 1PPH refined crystal structure, *@lic&* generated an alignment showing considerable superimposition of the common structural core whose amidine group formed, as was already observed with thrombin, a salt bridge with Asp189 of the highly conserved S1 region. R1 substituents were preferably located in the D subsite, whereas the R2 substituents were embedded in the area delimited by the S2 and P subsites. Unlike the thrombin model, CPCA indicated DRY, N1, and O as the most descriptive probes. DRY maps suggested that active compounds with hydrophobic and bulky R2 substituents, such as 3-benzylamidopiperidine and 4-benzylamidopiperidine of regioisomers **42** and **61**, respectively, were engaged in favorable hydrophobic interactions, indicated by cyan polyhedra, with Tyr94 and a large lipophilic cavity located between the P and S2 subsites. Active trypsin inhibitors (i.e., **9**) located lipophilic R1 substituents, such as β-naphthylsolphonyl, in a favorable cyan hydrophobic area on the D subsite. In a close region, the occurrence of unfavorable lipophilic yellow areas was likely

Table 4. The r^2_{pred} and ASPAR Values Calculated on the Training Set for the Three Serine Proteases through CoMSIA, COMBINE, and *@lic&* Methods

	CoMSIA			COMBINE			*@lic&*		
	thrombin	trypsin	fXa	thrombin	trypsin	fXa	thrombin	trypsin	fXa
r^2_{pred}	0.432	0.842	0.164	0.452	0.426	0.026	0.554	0.588	0.135
ASPAR	0.531	0.264	0.252	0.529	0.516	0.331	0.453	0.455	0.250

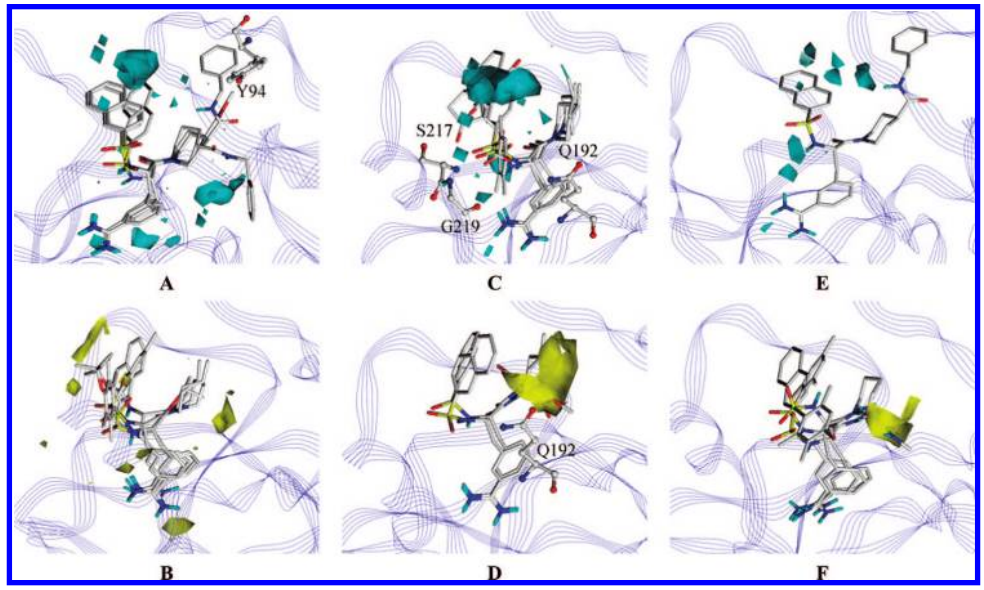

Figure 9. GRID maps for trypsin inhibitors. (A) DRY probe: favorable cyan areas were contoured at −0.00065 for active trypsin inhibitors **9** (pK_i = 7.444), **42** (pK_i = 6.921) and **61** (pK_i = 6.569). (B) DRY probe: unfavorable yellow areas were contoured at 0.00055 for inactive trypsin inhibitors **23** (pK_i = 5.398), **28** (pK_i = 5.854), **56** (pK_i = 4.854), and **62** (pK_i = 4.495). (C) N1 probe: favorable cyan areas were contoured at −0.0007 for active trypsin inhibitors **7** (pK_i = 6.201), **14** (pK_i = 7.131), and **26** (pK_i = 6.108). (D) N1 probe: unfavorable yellow areas were contoured at 0.0015 for inactive trypsin inhibitors **27** (pK_i = 5.658) and **60** (pK_i = 4.796). (E) O probe: favorable cyan areas were contoured at −0.0008 for active trypsin inhibitor **61** (pK_i = 6.569). (F) O probe: unfavorable yellow areas were contoured at 0.0019 for inactive trypsin inhibitors **59** (pK_i = 5.102), **68** (pK_i = 3.854), and **72** (pK_i = 3.00).

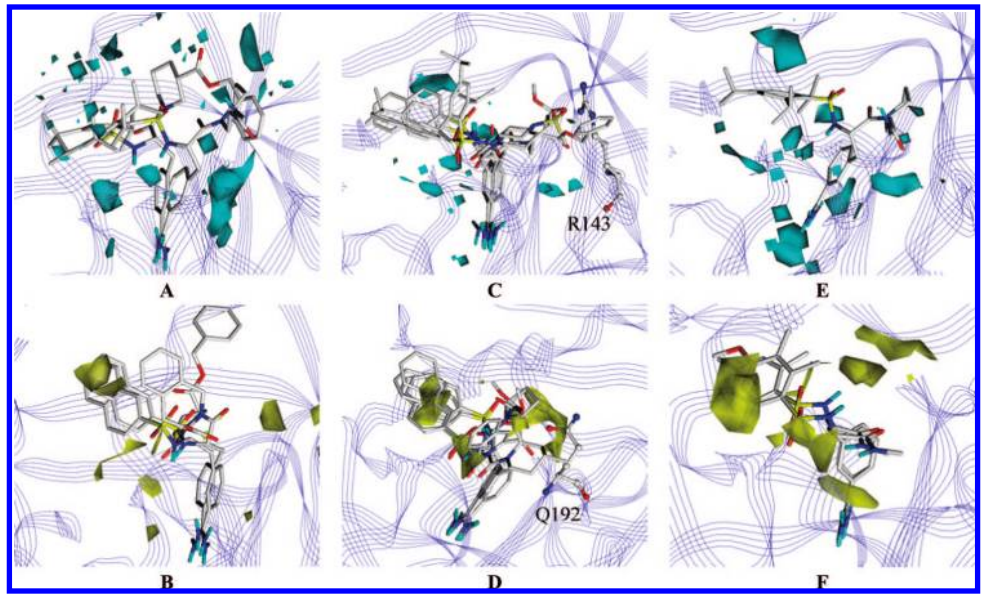

Figure 10. GRID maps for fXa inhibitors. (A) DRY probe: favorable cyan areas were contoured at −0.00075 for active fXa inhibitors **39** (pK_i = 5.824) and **54** (pK_i = 6.046). (B) DRY probe: unfavorable yellow areas were contoured at 0.00098 for inactive fXa inhibitors **10** (pK_i = 4.382) and **51** (pK_i = 4.699). (C) N1 probe: favorable cyan areas were contoured at −0.0007 for active fXa inhibitors **2** (pK_i = 5.167), **33** (pK_i = 5.585), **37** (pK_i = 5.092), and **41** (pK_i = 5.602). (D) N1 probe: unfavorable yellow areas were contoured at 0.0012 for inactive fXa inhibitors **27** (pK_i = 4.237), **29** (pK_i = 4.268), **52** (pK_i = 3.959), and **60** (pK_i = 3.886). (E) O probe: favorable cyan areas were contoured at −0.0005 for active fXa inhibitor **39** (pK_i = 5.824). (F) O probe: unfavorable yellow areas were contoured at 0.0011 for inactive fXa inhibitors **68** (pK_i = 3.731) and **72** (pK_i = 3.194).

due to the exposure of hydrophobic R1 chains of inactive inhibitors (i.e., **23**, **28**, **56**, and **62**) to the aqueous solvent.

The N1 GRID probe is particularly suitable for detecting HB acceptor groups. Interestingly, it was observed that HB

acceptor groups in R1, such as the carbonyl of anthraquinone **14** and the 4-methoxy group in **26** engaging in HBs with Ser217 and Gln192, respectively, impacted favorable cyan N1 map regions. Furthermore, as previously observed, Ser217 is an important structural determinant of trypsin selectivity, being mutated to Glu217 in both thrombin and fXa. In fact, this mutation replaces a HB donor group, serine OH, whose presence clearly explains the N1 favorable area, with the negatively charged HB acceptor carboxylate. Notably, these findings are in line with previous GRID investigations conducted with O and OS probes on the active sites of a large number of serine proteases.[44] The carbonyl group of the camphor ring of **7** established a HB with the backbone of Gly219, as indicated by a favorable cyan polyhedron. Conversely, the introduction of carbonyl or carboxyl groups in R2, as occurs in **27** and **60**, was detrimental for trypsin affinity, since they could impact with backbone and side-chain carbonyl groups of His57 and Gln192, respectively, both embedded in an unfavorable yellow area.

The O GRID probe looks for HB donor zones influencing target activity. To some extent, the results from this probe confirmed the observations made by examining N1 maps. Subsite S2 was unfavorable to HB donor ligands, such as the N-methylamide groups of **59**, **68**, and **72**, whose R2 substituents were embedded in an unfavorable yellow area. A slight recovery of affinity was observed for **61**, whose R2 substituent was rotated toward the outer part of the protein. Inhibitor **61** was about 10-fold more active toward trypsin than thrombin because its R2 chain was too bulky to fit into the additional P loop of thrombin.

3D QSAR Models for fXa Inhibition. Driven by the 1KYE refined crystal, the automated alignment obtained with our approach showed the R1 chains inserted into the D subsite, which, unlike trypsin and thrombin, revealed increased hydrophobicity for the incorporation of Tyr99 and Phe174, as already pointed out by other authors. Indeed, 5 of 9 of the most active fXa inhibitors bear the highly lipophilic 2,4,6-triisopropyl-phenylsolphonyl substituent at R1 directed toward the D subsite, whereas R2 groups generally seem to be oriented toward S1. As for trypsin, CPCA revealed DRY, N1, and O to be the most statistically significant informative probes. Owing to the lower affinity data and the narrower affinity range shown by fXa inhibitors compared to trypsin and thrombin, as a reasonable approximation, inhibitors with $pK_i > 5$ were considered to be active compared to those with $pK_i < 5$, which were assumed to be inactive when discussing GRID maps. Among the most active fXa inhibitors in the training set, R1 bulky and lipophilic substituents (i.e., 2,4,6-triisopropyl-phenylsolphonyl) of **39** and **54** impacted cyan-allowed accessible polyhedra in a cavity leaning on the D subsite whose more-pronounced hydrophobicity was already made evident. Their R2 substituents were very close to the S1 subsite and well-superimposed onto the RUP cocrystallized ligand. In contrast, inactive compounds, such as **10** and **51**, turned their substituents toward unfavorable areas, most likely those exposed to the solvent.

Favorable/unfavorable HB acceptor regions were detected by the N1 GRID probe. Active and moderately active inhibitors, such as **2**, **33**, and **37**, might be engaged in HB interactions with the Arg143 side chain while **41** interacts with the Gly218 backbone. Unfavorable zones for HB acceptor interactions were instead contoured by yellow polyhedra in the region between the S1 and S2 subsites, in proximity to the carboxylate, methoxy, and N-methylaminocarbonyl groups at position 2 of the piperidine/pirrolidine ring (i.e., **27**, **29**, **52**, and **60**), where the exposed carbonyl of Gln192 might impact HB acceptor groups of inactive compounds.

The O GRID probe was used to assess the effect of HB donor interactions. Favorable HB donor interactions can be ascribed to amidic substituents at position 3 of the piperidine ring of **39**, impacting a favorable cyan polyhedron. An opposite effect was observed for the HB donor NHMe groups of **68** and **72**, whose low affinity might also be due to the lower affinity of their R1 groups compared to the 2,4,6-triisopropyl-phenylsolphonyl substituents.

CONCLUSIONS

This investigation represents an effort to overcome some intrinsic limitations of 3D QSAR methods, in particular, the rational construction of molecular alignment and its effectiveness in explaining both binding affinity and molecular selectivity. Inside the receptors, docking was used to properly explore ligand conformational space, whose structure−activity potential was assessed by *@fit*, a novel fitness function. This function is the main feature of *@lic&*, an in-house-developed genetic algorithm. Through *@fit*, various ligand conformers, characterizing diverse ligand binding modes, may be adequately assessed and selected for subsequent molecular alignments. Unlike other approaches, three independent and diverse molecular overlays, derived from the selection of different conformers of the same ligand docked into the three diverse serine proteases, were analyzed through GRID/CPCA, which permitted the relation of their MIF variance with the distinct binding affinities for thrombin, trypsin, and fXa. The 3D QSAR models with robust statistics and simple and unbiased interpretability were obtained. Promising and, to some extent, more-reliable affinity predictions were observed using a multipoint equation which accounted for all of the docking poses using a weighting scheme. In addition, a satisfactory discrimination of selective inhibitors was also obtained and graphically explained by square plots. Our results were in conformity with and complemented those obtained in previous studies and modeling.[26,27] Of course, binding free energy postprocessing approaches, such as those based on molecular mechanics generalized Born-model solvent accessibility or molecular mechanics generalized Poisson−Boltzmann solvent accessibility methods,[59] would certainly furnish better energy descriptions of ligand binding compared to docking scores. At the same time, the extended linear response approach[60] might be an alternative, valuable, and rigorous tool for assessing selectivity as well as a deeper understanding of induced fit[61] due to the change of conformational degrees of freedom during the binding process. However, the use of these methods might be burdensome in terms of computational time. Similarly, the role of solvent should have deserved more attention, and indeed, runs of molecular dynamics would have been useful but perhaps unfeasible in managing the $3 \times 88 \times 20$ complexes analyzed in the present investigation. On the other hand, the use of docking software in addition to or as an alternative to GOLD

is currently being considered in an ongoing study, which also addresses the development of an automated tool to improve the detection of multiple binding modes that might strongly influence affinity and, even more, selectivity.

ACKNOWLEDGMENT

The authors wish to thank Dr. Paola Tedeschi and Dr. Ilenia Giangreco of MDM-L@b (Molecular & Data Modelling Laboratory), University of Bari, and DeLano Scientific LLC (540 University Ave., Ste. 325 Palo Alto, CA 94301-1928, U.S.A.) for their appreciated collaboration. Finally, the authors gratefully acknowledge the financial support from European Commission ("CancerGrid" STREP project, FP VI, Contract LSHC-CT-2006-03755) and MIUR (Rome, Italy; PNR project RBNE01F5WT).

Supporting Information Available: Scrambling analyses, determination of the minimum value of ASPAR for trypsin and fXa, selectivity studies for trypsin and fXa, numerical matrices containing docking scores and RMSD values, analyses of an additional molecular data set consisting of 54 coumarin MAO-B inhibitors along with statistics and predictions. This material is available free of charge via the Internet at http://pubs.acs.org.

REFERENCES AND NOTES

(1) Hansch, C.; Maloney, P. P.; Fujita, T.; Muir, R. M. Correlation of biological activity of phenoxyacetic acids with Hammett substituent constants and partition coefficients. *Nature* **1962**, *194*, 178–180.
(2) Cramer, R. D.; Patterson, D. E.; Bunce, J. D. Comparative Molecular Field Analysis (CoMFA). 1. Effect of shape on binding of steroids to carrier proteins. *J. Am. Chem. Soc.* **1988**, *110*, 5959–5967.
(3) Goodford, P. J. A computational procedure for determining energetically favorable binding sites on biologically important macromolecules. *J. Med. Chem.* **1985**, *28*, 849–857.
(4) Cruciani, G.; Pastor, M.; Mannhold, R. Suitability of molecular descriptors for database mining. A comparative analysis. *J. Med. Chem.* **2002**, *45*, 2685–2694.
(5) Sippl, W.; Cruciani, G. 3D-QSAR Using the GRID/GOLPE Approach. In *Molecular interaction fields. Application in drug discovery and ADME prediction*, 1st ed.; Wiley-VCH Verlag GmbH & Co. KGaA: Weinheim, Germany, 2006; *Vol. 27*, pp 145−165.
(6) Jewell, N. E.; Turner, D. B.; Willett, P.; Sexton, G. J. Automatic generation of alignments for 3D-QSAR analyses. *J. Mol. Graphics Modell.* **2001**, *20*, 111–121.
(7) Cho, S. J.; Sun, Y. FLAME: A program to flexibly align molecules. *J. Chem. Inf. Model.* **2006**, *46*, 298–306.
(8) Breu, B.; Silber, K.; Gohlke, H. Consensus adaptation of fields for molecular comparison (AFMoC) models incorporate ligand and receptor conformational variability into tailor-made scoring functions. *J. Chem. Inf. Model.* **2007**, *47*, 2383–2400.
(9) Doweyko, A. 3D-QSAR illusions. *J. Comput.-Aided Mol. Des.* **2004**, *18*, 587–596.
(10) Tropsha, A.; Grammatica, P.; Gombar, V. J. The importance of being earnest: validation is the absolute essential for successful application and interpretation of QSPR models. *QSAR Comb. Sci.* **2003**, *22*, 69–77.
(11) Jain, A. N.; Koile, K.; Chapman, D. Compass: predicting biological activities from molecular surface properties: Performance comparisons on a steroid benchmarks. *J. Med. Chem.* **1994**, *37*, 2315–2327.
(12) Mestres, J.; Rohrer, D. G. C.; Maggiora, G. MIMIC: a molecular-field matching program. Exploiting applicability of molecular surface approaches. *J. Comput. Chem.* **1997**, *18*, 934–954.
(13) Clark, R. D.; Strizhev, A.; Leonard, J. M.; Blake, J. F.; Matthew, J. B. Consensus scoring for ligand/protein interactions. *J. Mol. Graphics Modell.* **2002**, *20*, 281–295.
(14) Wang, R.; Lai, L.; Wang, S. Further development and validation of empirical scoring functions for structure-based binding affinity prediction. *J. Comput.-Aided Mol. Des.* **2002**, *16*, 11–26.
(15) Wei, H.; Tsai, K.; Lin, T. Modeling ligand-receptor interaction for some MHC class II HLA-DR4 peptide mimetic inhibitors using several molecular docking and 3D QSAR techniques. *J. Chem. Inf. Model.* **2005**, *45*, 1343–1351.
(16) Prathipati, P.; Saxena, A. K. Evolutionary of binary QSAR models derived from LUDI and MOE scoring functions for structure based virtual screening. *J. Chem. Inf. Model.* **2006**, *46*, 39–51.
(17) Berman, H. M.; Westbrook, J.; Feng, Z.; Gilliland, G.; Bhatt, N.; Shindyalov, I. N.; Bourne, P. E. The Protein Data Bank. *Nucleic Acid Res.* **2000**, *28*, 235–242.
(18) Nicolotti, O.; Miscioscia, T. F.; Leonetti, F.; Muncipinto, G.; Carotti, A. Screening of matrix metalloproteinases available from the PDB: insights into biological functions, domain organization and zinc binding groups. *J. Chem. Inf. Model.* **2007**, *47*, 2439–2448.
(19) Ferrara, P.; Gohlke, H.; Price, D. J.; Klebe, G.; Brooks, C. L., III. Assessing scoring functions for protein-ligand interactions. *J. Med. Chem.* **2004**, *47*, 3032–3047.
(20) Catto, M.; Nicolotti, O.; Leonetti, F.; Carotti, A.; Favia, A.; Soto-Otero, R.; Mendez-Alvarez, E.; Carotti, A. Structural insights into monoamine oxidase inhibitory potency and selectivity of 7-substituted coumarins from ligand- and target-based approaches. *J. Med. Chem.* **2006**, *49*, 4912–4295.
(21) Dorfman, R. J.; Smith, K. M.; Masek, B. B.; Clark, R. D. A knowledge-based approach to generating diverse but energetically representative ensembles of ligand conformers. *J. Comput. Aided Mol. Des.* **2007**, in press.
(22) Tuccinardi, T.; Ortore, G.; Rossello, A.; Supuran, C. T.; Martinelli, A. Homology modeling and receptor-based 3D-QSAR study of carbonic anhydrase IX. *J. Chem. Inf. Model.* **2007**, *47*, 2253–2262.
(23) Majeux, N.; Scarsi, M.; Apostolakis, C. E.; Caflisch, A. Exhaustive docking of molecular fragments with electrostatic solvation. *Proteins* **1999**, *37*, 88–105.
(24) Goldberg, D. E. *The Design of Innovation: Lessons from and for Competent Genetic Algorithms*; Kluwer Academic Publishers: Norwell, MA, 2002.
(25) Nicolotti, O.; Carotti, A. QSAR and QSPR studies of a highly structured physicochemical domain. *J. Chem. Inf. Model.* **2006**, *46*, 264–276.
(26) Böhm, M.; Stürzebecher, J.; Klebe, G. Three-Dimensional Quantitative Structure-Activity Relationship Analyses using Comparative Molecular Field Analysis and Comparative Molecular Similarity Indices Analysis to elucidate selectivity differences of inhibitors binding to trypsin, thrombin, and factor Xa. *J. Med. Chem.* **1999**, *42*, 458–477.
(27) Murcia, M.; Morreale, A.; Ortiz, A. R. Comparative binding energy analysis considering multiple receptors: a step toward 3D-QSAR models for multiple targets. *J. Med. Chem.* **2006**, *49*, 6241–6253.
(28) *SYBYL*, version 7.1; Tripos Inc: St. Louis, MO, 2007.
(29) Mohamadi, F.; Richards, N. G. J.; Guida, W. C.; Liskamp, R.; Lipton, M.; Caufield, C.; Chang, G.; Hendrikson, T.; Still, W. C. Macromodel: an integrated software system for modelling organic and bioorganic molecules using molecular mechanics. *J. Comput. Chem.* **1990**, *11*, 440–467.
(30) Brandstetter, H.; Turk, D.; Höffken, H. W.; Grosse, D.; Stürzebecher, J.; Martin, P. D.; Edwards, B. F.; Bode, W. Refined 2.3 Å X-ray crystal structure of bovine thrombine complexes formed with the benzamidine and arginine-based thrombin inhibitors NAPAP, 4-TAPAP and MPQA. A starting point for improving antithrombotics. *J. Mol. Biol.* **1992**, *226*, 1085–1099.
(31) Turk, D.; Stürzebecher, J.; Bode, W. Geometry of binding of the N^{α}-tosylated piperidines of m-amidino, p-amidino and p-guanidino phenylalanine to thrombin and trypsin. X-ray crystal structures of their trypsin complexes and modeling of their thrombin complexes. *FEBS Lett.* **1991**, *287*, 133–138.
(32) Mueller, M. M.; Sperl, S.; Stürzebecher, J.; Bode, W.; Moroder, L. (R)-3- Amidinophenylalanine-derived inhibitors of factors Xa with a novel active-site binding mode. *Biol. Chem.* **2003**, *383*, 1185–1191.
(33) *Maestro*, version 7.5.112; Schröedinger, LLC: New York, 2006.
(34) Jorgensen, W. L.; Maxwell, D. S.; Tirado-Rives, J. Development and testing of the OPLS All-atom force field on conformational energetics and properties of organic liquids. *J. Am. Chem. Soc.* **1996**, *118*, 11225–11236.
(35) Rice, P.; Longden, I.; Bleasby, A. EMBOSS: The European Molecular Biology Open Software Suite. *Trends Genet.* **2000**, *16*, 276–277.
(36) Ortiz, A. R.; Gomez-Puertas, P.; Leo-Macias, A.; Lopez-Romero, P.; Lopez-Viñas, E.; Morreale, A.; Murcia, M.; Wang, K. Computational approaches to model ligand selectivity in drug design. *Curr. Top. Med. Chem.* **2006**, *6*, 41–55.
(37) Morreale, A.; Gil-Redondo, R.; Ortiz, A. R. A new implicit solvent model for protein-ligand docking. *Proteins* **2007**, *67*, 606–616.
(38) Bhongade, B. A.; Gouripur, V. V.; Gadad, A. K. 3D-QSAR CoMFA studies on tyrpsin-like serine protease inhibitors: a comparative selectivity analysis. *Bioorg. Med. Chem.* **2005**, *13*, 2773–2782.
(39) Jones, G.; Willett, P.; Glen, R. C.; Leach, A. R. L.; Taylor, R. Development and Validation of a Genetic Algorithm for Flexible Docking. *J. Mol. Biol.* **1997**, *267*, 727–748.
(40) Nissink, J. W.; Murray, C.; Hartshorn, M.; Verdonk, M. L.; Cole, J. C.; Taylor, R. A new test set for validating predictions of protein-

ligand interaction. *Proteins* **2002**, *49*, 457–471.
(41) Verdonk, M. L.; Cole, J. C.; Hartshorn, M. J.; Murray, C. W.; Taylor, R. D. Improved protein-ligand docking using GOLD. *Proteins* **2003**, *52*, 609–623.
(42) Velec, H. F. G.; Gohlke, H.; Klebe, G. DrugScore CSD-knowledge-based scoring function derived from small molecule crystal data with superior recognition rate of near-native ligand poses and better affinity prediction. *J. Med. Chem.* **2005**, *48*, 6296–6303.
(43) Gillet, V. J.; Nicolotti, O. Evaluation of reactant-based and product-based approaches to the design of combinatorial libraries. *Perspect. Drug Discovery Des.* **2000**, *20*, 265–287.
(44) Kastenholz, M. A.; Pastor, M.; Cruciani, G.; Haaksma, E. E.; Fox, T. GRID/CPCA: a new computational tool to design selective ligands. *J. Med. Chem.* **2000**, *43*, 3033–3044.
(45) Pastor, M.; Cruciani, G. A novel strategy for improving ligand selectivity in receptor-based drug design. *J. Med. Chem.* **1995**, *38*, 4637–4647.
(46) Cruciani, G.; Watson, K. A. Comparative molecular field analysis using GRID force-field and GOLPE variable selection methods in a study of inhibitors of glycogen phosphorylase b. *J. Med. Chem.* **1994**, *37*, 2589–2601.
(47) Baroni, M.; Costantino, G.; Cruciani, G.; Riganelli, D.; Valigi, R.; Clementi, S. Generating Optimal Linear PLS Estimations (GOLPE): An Advanced Chemometric Tool for Handling 3D-QSAR Problems. *Quant. Struct.-Act. Relat.* **1993**, *12*, 9–20.
(48) Wold, S.; Trygg, J.; Berglund, A.; Antti, H. Some recent developments in PLS modeling. *Chemom. Intell. Lab. Syst.* **2001**, *58*, 131–150.
(49) Pastor, M.; Cruciani, G.; Clementi, S. Smart region definition: a new way to improve the predictive ability and interpretability of three-dimensional quantitative structure-activity relationships. *J. Med. Chem.* **1997**, *40*1455–1464.
(50) Nicolotti, O.; Gillet, V. J.; Fleming, P.; Green, D. A novel approach to deriving accurate and chemically intuitive QSAR models. *J. Med. Chem.* **2002**, *45*, 5069–5080.
(51) *MATLAB The Language Of Technical Computing*, version 7.3; The Mathworks: Natick, MA, 2006.
(52) *Pymol*, version 1.1beta3; Delano Scientific LLC: South San Francisco, CA, 2008.
(53) Hillebrecht, A.; Supuran, C. T.; Klebe, G. Integrated approach using protein and ligand information to analyze selectivity- and affinity-determining features of carbonic anhydrase isozymes. *ChemMedChem* **2006**, *1*, 839–53.
(54) Gnerre, C.; Catto, M.; Leonetti, F.; Weber, P.; Carrupt, P.; Altomare, C.; Carotti, A.; Testa, B. Inhibition of monoamine oxidases by functionalized coumarin derivatives: biological activities, QSARs, and 3D-QSARs. *J. Med. Chem.* **2000**, *43*, 4747–4758.
(55) Brühlmann, C.; Ooms, F.; Carrupt, P.; Testa, B.; Catto, M.; Leonetti, F.; Altomare, C.; Carotti, A. Coumarins derivatives as dual inhibitors of acetylcholinesterase and monoamine oxidase. *J. Med. Chem.* **2001**, *44*, 3195–3198.
(56) van Drie, J. H. Pharmacophore discovery - lessons learned. *Curr. Pharm. Des.* **2003**, *9*, 1649–1664.
(57) Wang, T.; Wade, R. C. Comparative binding energy (COMBINE) analysis of influenza neuramidase-inhibitor complexes. *J. Med. Chem.* **2001**, *44*, 961–971.
(58) Sheridan, R. P.; Holloway, M. K.; McGaughey, G.; Mosley, R. T.; Singh, S. B. A simple method for visualizing the differences between related receptor sites. *J. Mol. Graphics Modell.* **2000**, *43*, 3033–3044.
(59) Kalyanaraman, C.; Bernacki, K.; Jacobson, M. P. Virtual screening against highly charged active site: identifying substrates of alpha-beta barrel enzymes. *Biochemistry.* **2005**, *44*, 2059–2071.
(60) Tominaga, Y.; Jorgensen, W. L. General model for estimation of the inhibition of protein kinases using Monte Carlo simulations. *J. Med. Chem.* **2004**, *47*, 2534–2549.
(61) Nabuurs, S. B.; Wagener, M.; de Velig, J. A flexible approach to induced fit docking. *J. Med. Chem.* **2007**, *50*, 6507–6518.

CI800015S